Strong charge-transfer excitonic effects and Bose-Einstein exciton-condensate in graphane

Pierluigi Cudazzo[1], Claudio Attacalite[1], Ilya V. Tokatly[1,2] and Angel Rubio[1,3]
[1] *Nano-Bio Spectroscopy group and ETSF Scientific Development Centre, Dpto. Física de Materiales, Universidad del País Vasco, Centro de Física de Materiales CSIC-UPV/EHU-MPC and DIPC, Av. Tolosa 72, E-20018 San Sebastián, Spain*
[2] *IKERBASQUE, Basque Foundation for Science, E-48011 Bilbao, Spain*
[3] *Fritz-Haber-Institut der Max-Planck-Gesellschaft, Theory Department, Faradayweg 4-6, D-14195 Berlin-Dahlem, Germany*
(Dated: February 13, 2010)

Using first principles many-body theory methods (GW+BSE) we demonstrate that optical properties of graphane are dominated by localized charge-transfer excitations governed by enhanced electron correlations in a two-dimensional dielectric medium. Strong electron-hole interaction leads to the appearance of small radius bound excitons with spatially separated electron and hole, which are localized out-of-plane and in-plane, respectively. The presence of such bound excitons opens the path on excitonic Bose-Einstein condensate in graphane that can be observed experimentally.

Despite the short-live of graphene[1] and its derivatives the understanding and control of their properties rapidly approach a maturity[2, 3]. Chemical modifications by oxidation[4], functionalization and doping[5] have enhanced foreseen applications in nanotechnology. Recent synthesis of the fully hydrogenated-graphene (named "graphane")[6], which has been predicted to be a wide band-gap insulator with gap of 5.4 eV[7, 8], adds to the portfolio of carbon-based structures for nanodevice applications [3, 7]. The stability of the new 2D material has been analysed and two geometries (chair and boat) have been proposed[7]. However, there are still few open questions that need to be addressed: *i*) how much H is really incorporated in the samples? *ii*) does graphane inherit negative electron affinity of hydrogenated diamond samples used for electron-emitters? *iii*) what is the role of electron correlations in the band-structure and screening; are electron-hole effects as important as for carbon nanotubes[9–11] or small as in diamond[12]? The present letter address those issues, in particular the last three, by means of first-principles calculations based on many-body Green function theory. Our results indicate the possibility of having an excitonic Bose-Einstein condensate (BEC) by continuous pumping of excitons by light. Similar to the recent induced photoluminescence in graphene oxygenation[13], the strong spatial localization of the excitons in graphane points to a highly efficient defect-induced luminescence in chemically (or doped) modified graphane. In our ground state calculations of the most stable chair conformation of graphane (Fig.1 (b)) we used a pseudopotential plane-wave approach[14, 15] within the LDA approximation to DFT[16]. While excited states have been treated using the state-of-the-art many body approach[15, 17–19].

Before addressing the excitonic effects in the optical properties of graphane including the formation of BEC, we emphasize that although the dynamical stability of the ideal graphane in the chair conformation (Fig.1 (b)) has been recently shown[20], the calculated phonon spectra agrees only partially with the measured Raman data[6]. In particular the measured D peak agrees well with the calculated Raman active E_g phonon at 1340 cm^{-1} while the D' at 1620 cm^{-1} most likely originates from impurities as H vacancies. This means that there is a large defect density in graphane making it a hole-doped semiconductor with H vacancies acting as center for induced luminescence (see below). However at low doping H vacancies do not affect significantly the electronic structure, so that ideal graphane allows to obtain a realistic description of the electronic and optical properties of this system. On the other hand, the stability of graphane as hole-doped semiconductor, suggests the possibility to achieve a metallic phase under strong hole-doping by dehydrogenation. In this conditions we have a strong electron-phonon renormalization of the phonon frequencies around the BZ center (Kohn-anomaly)[15]. Similar to the case of doped diamond[24], this is a manifestation of a strong electron-phonon coupling pointing to the possibility of having a high T_c superconducting phase.

Electronic properties: the band structure of graphane (Fig.1 (c)) is mainly dictated by the sp^3 hybridization of carbon orbitals (see Fig. 1 (b)). This causes a band gap opening (3.4 eV at the DFT-Kohn-Sham level) with respect to graphene. The classification of states is especially simple at the Γ-point. The top/bottom valence$(E_g)/(A_{1g})$ corresponds to the C-C bonding σ states, while two intermediate occupied bands corresponds to C-H bonding σ states (A_{1g}). The bottom of the conduction band is the anti-bonding A_{2u} C-H σ state and the anti-bonding E_u C-C σ state appears at higher energy (2.00 eV). The other bands correspond to free-electron-like states. Electron self-energy effects computed at the GW-level[15, 17, 19] modify strongly the band structure (red dots on Fig.1 (c)): the fundamental energy gap at Γ increases from 3.4 eV to 5.4 eV, while the gaps at the high

symmetry points M and K become 14.2 eV and 15.9 eV, instead of LDA values of 10.6 eV and 11.8 eV, in agreement with recent calculations[8]. Moreover we found that the vacuum level is at about 4.9 eV from the top of the LDA valence band (see Fig.1 (c)) so that graphane has a positive electron affinity both in LDA (1.44 eV) and GW (0.66 eV).

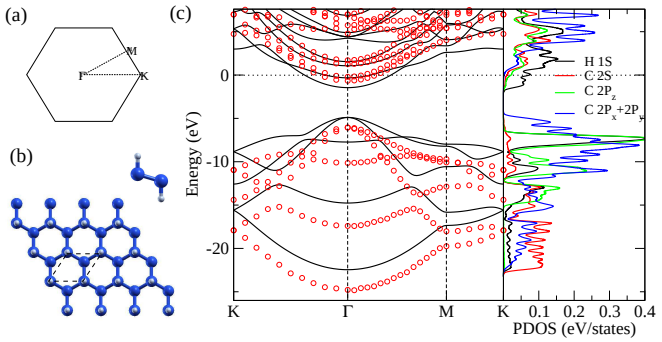

FIG. 1: First Brillouin zone (a) and unit cell and bases of graphane in the chair conformation (b). Blue and white balls represent carbon and hydrogen atoms respectively. (c) Band structure in LDA (full line) and GW approximation (red circles) and projected density of states of graphane. The zero indicates the vacuum level position.

Optical properties of graphane: In Fig.2 we plot the imaginary part of the macroscopic dielectric function $\epsilon_M(\omega)$ for a light propagating along the graphane plane in the x-direction. To reveal the physical origin of different features in the optical spectrum we compare $\mathrm{Im}\epsilon_\mathrm{M}(\omega)$ calculated (i) without taking into account both the inter-electron and the electron-hole correlations, LDA-RPA, that is the random phase approximation (RPA) on top of the bare LDA band structure, (ii) RPA using the *GW* quasi-particle spectra (GW-RPA) which neglects electron-hole correlations, and, finally, (iii) from the full solution of the Bethe Salpeter equation (BSE) which accounts the excitonic effects[15, 18, 19].

The LDA-RPA absorption spectrum (green line in Fig.2) do not show any significant feature near to the LDA band gap (3.4 eV) because the corresponding transitions, being dipole-allowed, have small oscillator strength as the overlap between the top-valence (localized on the C-C bond,) and bottom-conduction (localized on the C-H bond) states is small. Pronounced features in $\epsilon_M(\omega)$ are present at higher energies. The peak about 8.5 eV is related to vertical transitions from the valence band to the conduction band at large wave vectors, while the peak at 10.2 eV corresponds to transitions near to the M point. The large structure at 11.2 eV arise from a Van Hove singularity near M corresponding to transitions from the valence band to out-of-plane states with Kohn-Sham energies between 3.37 eV and 4.14 eV. The main effect of the quasi-particle corrections is a strong global shift of the absorption spectrum to higher energies (GW-RPA curve in Fig.2). Since the optical transition energy increases the amplitude of $\epsilon_M(\omega)$ is reduced to satisfy the f-sum rule. However, we show that electron-hole correlations dramatically modify the shape of $\epsilon_M(\omega)$ (see BSE curve in Fig.2). The "bulk" of the absorption spectrum nearly comes back to the original LDA-RPA position, but with a significant redistribution of the oscillator strengths from the higher to the lower energies, and an appearance of a number of pronounced excitonic resonances that are related to electron-hole pairs with electrons in the delocalized out-of-plane states[15].

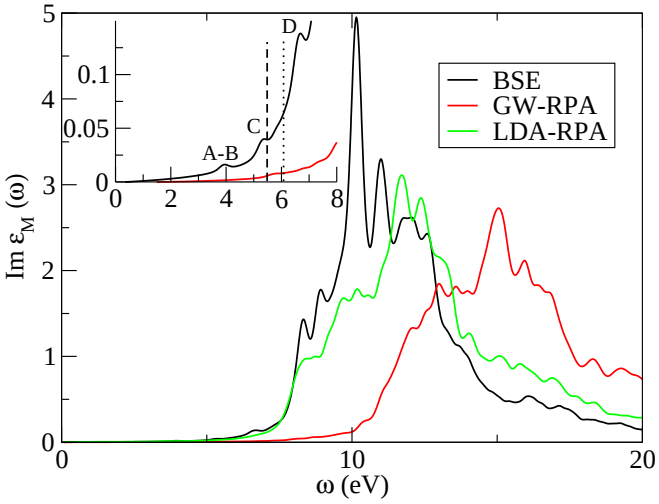

FIG. 2: Imaginary part of the macroscopic dielectric function for light polarized along the graphane plane. The dashed and dotted lines in the inset indicate the position of the GW gap and vacuum level respectively. For light propagating along the z axes the spectrum (not shown) is flat up to 8 eV.

In this work we concentrate on the most prominent physical effect of the electron-hole interactions in graphane, the appearance of bound excitons below the GW gap (see inset in Fig.2). These excitations, which are completely missing in RPA, are responsible for the UV absorption of graphane. The absorption spectrum for light propagating along x shows two bound excitons (B and C) with large binding energies of 1.6 eV and 0.3 eV, respectively. The solution of the BS equation also reveals the existence of a dark exciton (A), 2 meV below the first optically active B-exciton. The exciton C is related to transitions from the highest valence band to the first out-of-plane band and its wave function is delocalized out-of-plane[15]. In contrast, the spatial extension of the strongly bound excitons A and B is very small, $r_{ex} \approx 5.0$ Å, as it can be seen in Fig.3 (b) and (d). These excitons are formed from the states of the double degenerate (at Γ-point) E_g valence band and the A_{2u} conduction band (the hole states in these excitons belong to the lowest, $\mathrm{E}_g^{(2)}$, and the highest, $\mathrm{E}_g^{(1)}$, bands respectively). Their wave functions reflect the C-H anti-bonding character of the states with the electron mainly

localized on top of the H-atoms. Since the hole is localized on the C-C bonds, the creation of such excitons corresponds to a charge transfer from the middle of the carbon plane to the side planes on top of the hydrogen atoms (see Fig.3 (a) and (c)).

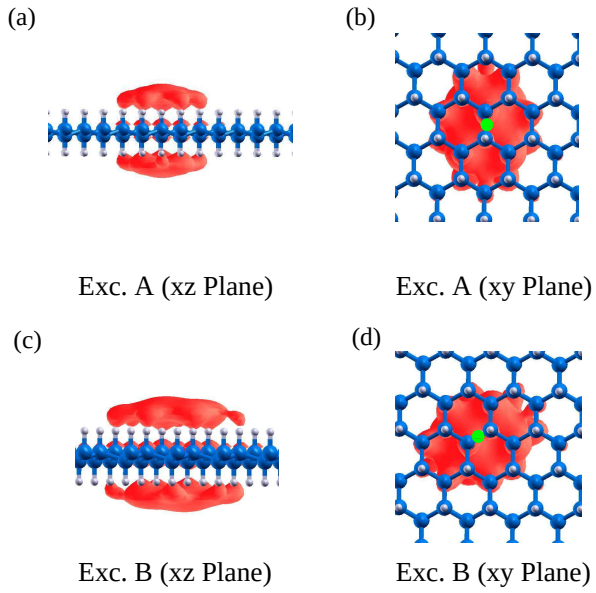

FIG. 3: 3D-Shape of the low energy excitons wave function for fixed position of the hole (green circle).

It is instructive to compare absorption spectra of graphene[22] and graphane. Electron-hole interaction is important in both systems. However, in the former it leads only to a redistribution of the oscillator strength resulting in the appearance of a resonant exciton at 4.5 eV, while in the latter it gives rise to a strongly bound exciton at 3.8 eV where the spectrum of graphene is completely flat. This can be used as an additional experimental fingerprint of the presence of hydrogenated platelets embedded in graphene.

Considering the light propagating in the y-direction we find that the role of the strongly bound excitons is inverted: A exciton becomes optical active, while B exciton is dark. Since the two excitons are nearly degenerate and have identical oscillator strengths for the corresponding polarization of light the absorption spectra remain almost unchanged. The reason for this is the symmetry of Bloch states involved in the formation of the excitons: the electronic states have A_{2u} symmetry, while the hole states belong to the 2D irreducible representation E_g with the eigenfunctions $\psi^{(1)}_{E_g}$ and $\psi^{(2)}_{E_g}$. A group theoretical analysis[15] shows that the only nontrivial dipole matrix elements are: $\langle\psi_{A_{2u}}|x|\psi^{(1)}_{E_g}\rangle$ and $\langle\psi_{A_{2u}}|y|\psi^{(2)}_{E_g}\rangle$, which explains why the A and B excitons are only visible for the y- and x-polarization, respectively. For the light propagating perpendicular to the graphene plane both excitons are dipole forbidden.

The presence of H-vacancies with the strong spatial localization of the lowest A-exciton makes graphane to luminescence with high yield upon UV excitations, similarly to layered h-BN where a high luminescence yield is observed from a strong localized exciton[23].

A striking feature of the excitons A and B is their large binding energy, which at least by an order of magnitude exceeds that in typical wide gap semiconductors. This becomes especially surprising if we note that both the A_{2u} conduction band and the E_g valence bands are nearly perfect parabolas over a large fraction of BZ, and, therefore, the excitons, despite their small radius, should be reasonably well described within the effective mass approximation. Using the standard method of invariants [25] we derived the $\mathbf{k}\cdot\mathbf{p}$ Hamiltonian at Γ for the valence bands

$$\hat{H}(\mathbf{k}) = \alpha\hat{I}(k_x^2+k_y^2) + \beta[\hat{\sigma}_z(k_x^2-k_y^2) + 2\hat{\sigma}_x k_x k_y], \quad (1)$$

and for the conduction band $\hat{H}(\mathbf{k}) = \frac{k_x^2+k_y^2}{2m_e}$[15], from which we find the value of the reduced electron-hole mass $\mu_{ex} = 0.29m_0$, which is very typical for most known semiconductors (here m_0 is the bare electron mass, and for simplicity we model the two valence bands by a single parabola with an average mass). A resolution of the apparent paradox is an unusual form of the effective electron-hole interaction in graphane. In 3D dielectric media the effective interaction is obtained by the replacement $e^2/r \to e^2/\epsilon r$, where ϵ is the static dielectric constant. This simple recipe does not work in graphane that is a 2D dielectric, where the very notion of the dielectric constant makes no sense. In fact, an external electric field E induces a polarization P which is bound to the plane: $P(\mathbf{r}) = \alpha_{2D}E(\mathbf{r})\delta(z)$, where α_{2D} is the internal polarizability of the 2D dielectric. Using the above relation in the Poisson equation for a point charge we get the following effective interaction potential (its 2D Fourier component)

$$V_{eff}(\mathbf{q}) = \frac{2\pi e^2}{|\mathbf{q}|(1+2\pi\alpha_{2D}|\mathbf{q}|)} \quad (2)$$

which is very different from the trivial renormalization of charge in 3D systems. The only parameter entering Eq.2 is the polarizability α_{2D} of a single graphane layer, which we extract from our *ab initio* results. Since our calculation are performed for a periodic stack of layers with sufficiently large inter-layer distance L, the 2D polarizability is related to the actually calculated 3D polarizability as follows $\alpha_{2D} = L\frac{\epsilon-1}{4\pi}$, where ϵ is the dielectric constant of our 3D multilayer system. We can also estimate the exciton binding energy E_{ex} by the variational solution of the Schrödinger equation with the effective potential in Eq.2 using the simplest trial wave function, $\psi \sim e^{-r/a}$, where a is the variational parameter[26]. The result $E_b = 2.0$ eV is very close to the ab-initio value

of 1.6 eV, while the optimized value of the variational parameter $a = 7.7$a.u. almost perfectly matches the actual excitonic radius. Hence we clearly see that unusual strong binding of excitons in graphane is a result of a weak and specifically nonlocal 2D dielectric screening.

Because of the small radius and the large binding energy of excitons it is tempting to consider graphane as a potential candidate for a realization of the Bose-Einstein condensation (BEC) of optically pumped excitons. Indeed, using the standard expression for the degeneracy temperature T_0 of a 2D Bose gas[27]:

$$k_B T_0 = \frac{2\pi\hbar^2 n}{M_{ex}} \tag{3}$$

(here $M_{ex} = m_c + m_v \approx 1.3 m_0$ is the excitonic mass) we find that at room temperature $T_0 = 300K$ the quantum degeneracy of excitonic gas in graphane is reached for the density $n \approx 5\ 10^{12}\text{cm}^{-2}$, which is two orders of magnitude smaller than $\frac{1}{\pi a_{ex}^2} = 5.1\ 10^{14}\text{cm}^{-2}$ (the later value sets an order of magnitude of the Mott critical density for the transition from the gas of excitons to a gas/liquid of unbound electrons and holes). Another argument in favor of excitonic BEC in graphane is a spatial separation of the charges in the excitonic state – the hole is localized in the middle C-layer, while the electron on top of the H-layers. Therefore graphane looks quite similar to the coupled quantum wells (CQW) structures, which are very popular for experiments on excitonic BEC [28, 29]. In CQW [28, 29] such a separation leads to a very long excitonic life time that reaches microseconds. To estimate the radiative life time τ of the excitons in graphane we adopted a 2D version of the approach of Ref.[30], which lead to the following relation

$$\frac{1}{\tau} = \frac{4\pi e^2 \Omega}{\hbar c} \frac{d^2}{A}, \tag{4}$$

where Ω, d and A are the exciton frequency, dipole matrix element, and the unit cell area, respectively. The result we find, $\tau = 15$ ps, is not very encouraging – the value is too small to unconditionally speak about BEC. On the other hand, it is still larger that the lifetime of cavity polaritons where BEC has probably been observed [31]. Clearly a detailed analysis of the thermalization kinetics is needed to make more definite predictions. Defects will also play a role in pinning the exciton condensate. Nonetheless, we believe that BEC of strongly bound, small radius excitons in graphane is an interesting possibility which deserves to be carefully studied both experimentally and theoretically.

This work was supported by the Spanish MEC (FIS2007-65702-C02-01), ACI-Promociona (ACI2009-1036) Grupos Consolidados UPV/EHU del Gobierno Vasco" (IT-319-07), the European Union through e-I3 ETSF project (Contract Number 211956). We acknowledge support by the Barcelona Supercomputing Center, Red Espanola de Supercomputacion".

[1] K. S. Novoselov, *et al.*, Science **306**, 666 (2004)
[2] A. K. Geim, Science **323**, 1530 (2009).
[3] A. K. Geim and K. Novoselov, Science **324**, 875 (2009).
[4] R. Ruoff, Nature **3**, 10 (2008).
[5] X. Wang, *et al.*, Science **324**, 768 (2009).
[6] D. C. Elias, *et al.*, Science, **323**, 356 (2008).
[7] J. O. Sofo, A. S. Chaudhari and G. D. Baber, Phys. Rev. B **75**, 153401 (2007).
[8] S. Lebégue, M. Klintenberg, O. Eriksson and M. I. Katsnelson, Phys. Rev. B **79**, 245117 (2009).
[9] C. D. Spartaru, S. Ismail-Beigi, L. X. Benedict and S. G. Louie, Phys. Rev. Lett. **92**, 077402 (2004).
[10] F. Wang, G. Dukovic, L. B. Brus and T. F. Heinz, Science **308**, 838 (2005).
[11] E. Chang, G. Bussi, A. Ruini and E. Molinari, Phys. Rev. Lett. **92**, 196401 (2004).
[12] A. Marini, R. Del Sole and A. Rubio, Phys. Rev. Lett. **91**, 256402 (2003).
[13] T. Gokus, R. R. Nair, A. Bonetti, M. Bohmier, A. Lombardo, K. S. Novoselov, A. K. Geim, A. C. Ferrari and A. Hartschuh, ACS Nano. **3(12)**, 3963 (2009).
[14] S. Baroni, A. Dal Corso, S. de Gironcoli and P. Giannozzi, http://www.pwscf.org.
[15] See EPAPS Document No [] for [a description of Numerical details, Symmetry properties of the wave functions, Analysis of the excitonic resonances in graphane absorption spectra of Fig.2, Phonon spectra and $\mathbf{k}\cdot\mathbf{p}$ Hamiltonian].
[16] W. Kohn and L. J. Sham, Phys. Rev. **140**, A1133 (1965).
[17] L. Hedin, Phys. Rev. **139**, A796 (1965).
[18] G. Onida, L. Reining and A. Rubio, Rev. Mod. Phys. **74**, 601 (2002).
[19] A. Marini, C. Hogan, M. Grüning and D. Varsano, *Computer Physics Communications* **180**, 1392 (2009).
[20] H. Sahin, C. Ataca and S. Ciraci, Appl. Phys. Lett. **95**, 222510 (2009).
[24] K. W. Lee and W. E. Pickett, Phys. Rev. Lett. **93**, 237003 (2004).
[22] L. Yang, J. Deslippe, C. H. Park, M. L. Cohen and S. G. Louie, Phys. Rev. Lett. **103**, 186802 (2009).
[23] K. Watanabe, T. Taniguchi and H. Kanda, Nature **3**, 404-409 (2004).
[24] K. W. Lee and W. E. Pickett, Phys. Rev. Lett. **93**, 237003 (2004).
[25] G. L. Bir and G. E. Pikus, *Symmetry and strain-induced effects in Semiconductors*, (Wiley, New York), 1974.
[26] Cudazzo, P., *et. al.* In preparation.
[27] S. A. Moskalenko and D. W. Snoke, *Bose-Einstein Condensation of Excitons and Biexciton* (Cambridge Univ. Press, Cambridge, 2000)
[28] L. V. Butov, *et al.*, Nature **417**, 47-52 (2002).
[29] D. W. Snoke, *et al.*, Nature **418**, 754-757 (2002).
[30] C. D. Spartaru, S. Ismail-Beigi, R. B. Capaz and S. G. Louie, Phys. Rev. Lett. **95**, 247402 (2005).
[31] J. Kasprzak, *et al.*, Nature **443**, 409-414 (2006).

Supplementary material

(Dated: February 13, 2010)

NUMERICAL DETAILS

Our calculations of the ground state properties are based on density functional theory[1, 2] (DFT) within local density approximation[3] (LDA) implemented in the pseudo-potential plane wave framework[4]. The chair conformation has been simulated using a two dimensional triangular lattice with a basis of two CH units where the ionic potential has been modeled using Bachelet, Hamman and Schlüter pseudopotentials[5]. The distance between two adjacent layers has been set to 15Å to simulate an isolated Graphane sheet. We chose a 90 Ry kinetic energy cutoff for the electronic wave function expansion and a $16 \times 16 \times 1$ Monkhorst-Pack[6] mesh for Brillouin zone (BZ) integration. Then, the optimized unit cell has been obtained minimizing the total energy as a function of the lattice parameter. At each value of the lattice constant the atomic positions (*i.e.* the internal degree of freedom) were fully relaxed to minimize the Hellman-Feynman[7] forces. In the optimized structure the two CH units relax up-word and down-word respect to the ideal position of the graphene layer resulting in the formation of sp^3 C-C and C-H bonds. In particular the bond length are 1.51 Å (for the C-C bonds) and 1.11 Å (for the C-H bonds) in agreement with previous calculations[8, 9].

Phonon frequencies were calculated using the plane waves method within Linear Response Theory[10] using a $30 \times 30 \times 1$ Monkhorst-Pack k-point mesh to compute the dynamical matrix. This allows us to achieve a very good convergence on the phonon spectrum (about 2% in the phonon frequency). A $10 \times 10 \times 1$ q-mesh in the BZ was used to interpolate the force constants for the phonon dispersion calculation.

Finally in calculating the QP energies we used the GW approximation of Hedin[11, 12], and the Bethe-Salpeter equation (BSE) has been solved to cope with excitonic effects in the absorption spectra[12, 13]. In particular in our calculation of QP energies we used a $30 \times 30 \times 1$ k-point mesh and 100 bands for computing the self energy. We take into account dynamical screening effects in W through the generalized plasmon pole model. The same k-point mesh with 40 bands has been used to evaluate the dielectric function in RPA. The electron-hole kernel in the BSE and the dielectric function has been evaluated on a $30 \times 30 \times 1$ k-point mesh. Moreover we used 100 bands for the calculation of W and 20 bands to evaluate $\epsilon_M(\omega)$ since we were interested to the low energy region of the spectrum.

PHONON SPECTRA FOR PURE AND DOPED GRAPHANE

In Fig.1 (solid line) we show the calculated phonon dispersion curve for a perfect graphane in the chair configuration. The phonon spectra presents three well separated types of vibrations: the low-frequency acoustic modes (not shown), the intermediate-frequency optical modes involving the stretching of the C-C bonds, and separated by a gap of 1500 cm^{-1} (not shown), we find optical modes corresponding to C-H bonds. The presence of this large gap proves that the vibrations of H atoms are almost completely decoupled from the other modes.

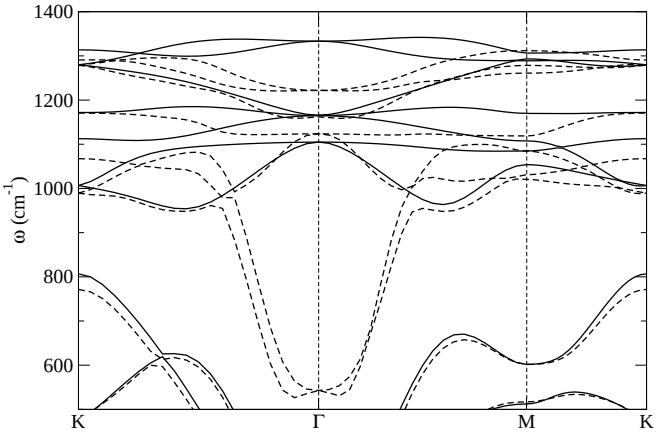

FIG. 1: Phonon spectra of ideal (solid line) and 1% hole-doped (dasched line) graphane in the chair conformation

.

Comparison of our calculated spectra with available experimental Raman data, shows that the measured D peak agrees well with the calculated Raman active E_g phonon at 1340 cm^{-1} while the D' peak observed at 1500 cm^{-1} most likely is related to impurity effects due to H vacancies.

Finally, in Fig.1 we compare the phonon spectra of ideal graphane (solid line) with that of 1% hole-doped graphane (dashed line) obtained in the rigid-band approximation. As we can see hole-doping causes a strong renormalization of the phonon spectra near to the Γ point. In particular the two degenerate optical modes related to the C-C stretching with H atoms moving in-phase with C atoms soften from 1168 cm^{-1} to 542 cm^{-1} while the two degenerate optical modes related to C-C stretching with H atoms moving out-of-phase with C atoms soften from 1333 cm^{-1} to 1221 cm^{-1}. The large Kohn anomaly at 340 cm^{-1} suggest a strong electron-phonon coupling in doped graphane related to the C-C covalent bonds. This makes doped graphane a possible

candidate for high T_c superconductivity.

SYMMETRY PROPERTIES OF THE WAVE FUNCTIONS

In this section we perform an analysis of symmetry properties of the wave functions corresponding to the valence and conduction bands at the Γ point based on the group theory. This allows to explain the behaviour of the absorption spectra at low energy for different polarizations and the nature of the two nearly degenerate excitons.

Graphane in the chair conformation belongs to the D_{3d} point group which is characterized by 12 symmetry operations (with inversion) and 6 irreducible representations: two 2D representations E_g and E_u and four 1D representations A_{1g}, A_{2g}, A_{1u} and A_{2u} (see table I).

	E	$2C_3$	$3C_2'$	i	$2S_6$	$3\sigma_d$	Basis functions
A_{1g}	1	1	1	1	1	1	x^2+y^2, z^2
A_{2g}	1	1	-1	1	1	-1	
E_g	2	-1	0	2	-1	0	(x^2-y^2, xy) (xz, yz)
A_{1u}	1	1	1	-1	-1	-1	
A_{2u}	1	1	-1	-1	-1	1	z
E_u	2	-1	0	-2	1	0	(x, y)

TABLE I: Character table for D_{3d} point group.

Since the valence bands are two fold degenerate at the Γ point they belong to one of the 2D irreducible representation E_g or E_u. However as can be inferred from Fig.2 (a) and (c), the wave functions corresponding to the valence bands are symmetric respect to the inversion. This is sufficient to conclude that the valence bands indicated with $\epsilon^{(1)}_{E_g}$ and with $\epsilon^{(2)}_{E_g}$ belong to the E_g irreducible representation. Moreover we indicate with $\psi^{(1)}_{E_g}$ and $\psi^{(2)}_{E_g}$ the corresponding wave function, with the label 1(2) indicating that the wave function is antisymmetric (symmetric) under reflection respect to the YZ plane.

The conduction band is not degenerate and it is characterized by a wave function antisymmetric respect to the inversion (see Fig.2 (b)). On the other hand this latter is antisymmetric under refection respect to the YZ plane. Thus the conduction band ($\epsilon_{A_{2u}}$) belongs to the A_{2u} (see tableI) irreducible representation.

Now we focus on the symmetry properties of a general polar vector (x, y, z) as for example the dipole moment. It can be easily shown that the third component z transforms in agreement with the A_{2u} irreducible representation, while the in-plane components (x, y) transform in agreement with the E_u irreducible representation. In particular y is the partner of x. Then, when the light is directed along the Z axis the possible states coupled with the valence bands by dipole moment are contained in the direct product $A_{2u} \times E_g = E_u$. This means that transitions from the valence to the conduction bands are forbidden for light directed along the Z axis and both excitons A and B are not visible. On the other hand, when the light is directed along X or Y, the possible states coupled with the valence bands by dipole moment are contained in the direct product $E_u \times E_g = A_{1u} + A_{2u} + E_u$ which is a 4D reducible representation of the symmetry group in the bases defined by the four wave functions: $x\psi^{(1)}_{E_g}$, $y\psi^{(1)}_{E_g}$, $x\psi^{(2)}_{E_g}$ and $y\psi^{(2)}_{E_g}$. It is now possible, starting from this bases set, to generate a set of wave functions symmetrically adapted with the three irreducible representation appearing in the direct product $E_u \times E_g$. In particular we found that the only wave function which transform in agreement with the A_{2u} irreducible representation is a linear combination of $x\psi^{(2)}_{E_g}$ and $y\psi^{(1)}_{E_g}$. This means that the only possible transitions involving the wave function $\psi_{A_{2u}}$ are: $\langle\psi_{A_{2u}}|x|\psi^{(1)}_{E_g}\rangle$ and $\langle\psi_{A_{2u}}|y|\psi^{(2)}_{E_g}\rangle$.

It is now clear why the most bounded exciton related to electron-hole pairs $(\psi_{A_{2u}}, \psi^{(2)}_{E_{2g}})$ is optical active for light polarized along Y, while the highest energy exciton related to electron-hole pairs $(\psi_{A_{2u}}, \psi^{(1)}_{E_{2g}})$ is visible for light polarized along X. However, due to the small overlap between $\psi_{A_{2u}}$ and ψ_{E_g} wave functions the two excitons present a very small strength compared with that

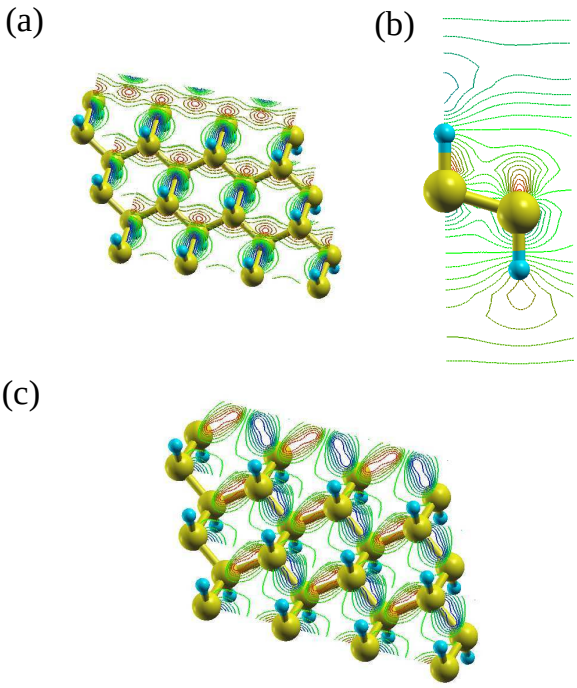

FIG. 2: Projection on the XY ((a) and (c)) and ZY (b) planes of the wave functions $\psi^{(2)}_{E_{2g}}(\mathbf{r})$ (a), $\psi_{A_{2u}}(\mathbf{r})$ (b) and $\psi^{(1)}_{E_{2g}}(\mathbf{r})$ (c). The red-blue lines refer to negative-positive values of the wave function.

of the higher energy excitons. As a results, it does not reflect with evident features on the behaviour of $\epsilon_M(\omega)$.

ANALYSIS OF THE EXCITONIC RESONANCES IN THE GRAPHANE ABSORPTION SPECTRA OF FIG.2

The prominent peak at 15.4 eV is completely depressed, while the absorption is strongly enhanced at 10.2 eV and 11.0 eV. The first peak at 10.2 eV is related to the correlated electron and hole states with large wave vectors from the E_g bands and out-of-plane bands with QP energies 0.9 eV $\leq \epsilon^{QP}_{n\mathbf{k}} \leq$ 2.1 eV. The "binding energy" is about 0.5 eV. The second resonant exciton at 11.0 eV has a lower binding energy (0.2 eV) and is formed by electron-hole pairs from C-H valence states and out-of-plane states with QP energy close to 1.20 eV. The series of excitonic resonances between 8.30 eV and 8.90 eV are related to the electron-hole pairs corresponding to transitions from the small wave vector E_g states to the out-of-plane states with QP energies 0.13 eV$\leq \epsilon^{QP}_{n\mathbf{k}} \leq$ 2.02 eV. Finally, the lowest resonant excitonic peak at 6.46 eV (peak D in the inset in Fig.2) originates from the mixture of the transitions from the highest E_g valence band to the A_{2u} conduction band and the first out-of-plane band. Because of the free-electron character of the electronic states involved in all these electron-hole resonances the corresponding excitonic wave functions are completely delocalized in the out-of-plane regions (see Fig.3 (b)).

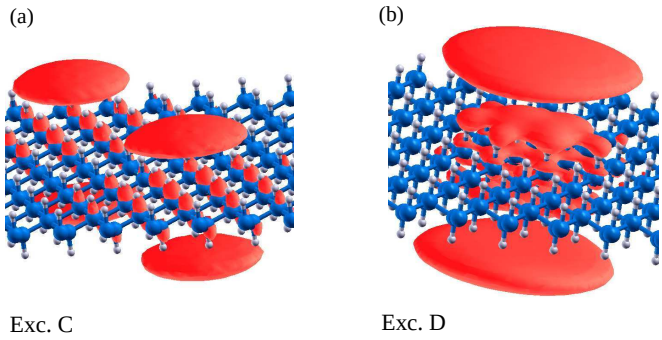

FIG. 3: 3D-Shape of the excitonic wave function for the exciton C (a) and D (b).

$\mathbf{k}\cdot\mathbf{p}$ HAMILTONIAN

In this section we derive the $\mathbf{k}\cdot\mathbf{p}$ Hamiltonian $\hat{H}(\mathcal{K})$ for the valence bands around the Γ point ($\mathcal{K}$ being a second order tensor operator which depends from the components of the wave vector $\mathbf{k}$). To determine the number of the independent parameters in $\hat{H}(\mathcal{K})$ we use the method of the invariants[14], which consists to impose the condition:

$$\hat{D}^{E_g}(g)\hat{H}(g^{-1}\mathcal{K})\hat{D}^{E_g^{-1}}(g) = \hat{H}(\mathcal{K}) \tag{1}$$

for each transformation g of the symmetry group. $\hat{D}^{E_g}(g)$ being the 2D matrix representing g in the E_g irreducible representation.

Since the matrix Eq.1 represents $N^2 = 4$ equations for the elements $\hat{H}_{ij}(\mathcal{K})$ of $\hat{H}(\mathcal{K})$, these constraints allow one to construct $\hat{H}(\mathcal{K})$.

To determine the correct form of the Hamiltonian, we first note that the tensor operator $\mathcal{K}$ can be decomposed into two irreducible tensor operators, one ($\mathcal{K}^{A_{1g}} = k_x^2 + k_y^2$) belonging to the A_{1g} irreducible representation and one ($\mathcal{K}^{E_g} = (k_x^2 - k_y^2, 2k_xk_y)$) belonging to the E_g irreducible representation ($2k_xk_y$ being the partner of $k_x^2 - k_y^2$). Furthermore, $\hat{H}(\mathcal{K})$ can be decomposed on a complete set of linearly independent 2×2 dimensional matrices that transform according to those irreducible representations which are contained in the direct product $E_g \times E_g = E_g + A_{1g} + A_{2g}$. Starting from the four linearly independent matrices $\hat{I}$ (identity matrix), $\hat{\sigma}_x$, $\hat{\sigma}_y$ and $\hat{\sigma}_z$ (Pauli matrices) we can construct a set of linearly independent matrices $\hat{\chi}_1^\Gamma$ symmetrically adapted with the irreducible representation $\Gamma = E_g, A_{1g}, A_{2g}$. This can be done in terms of the standard group theory using the relation:

$$\hat{\chi}_1^\Gamma = \sum_g \hat{D}^{E_g}(g)\hat{\chi}\hat{D}^{E_g^{-1}}(g)D^\Gamma_{11}(g) \tag{2}$$

where $\hat{\chi}$ runs on the four matrices (*i.e.* the identity and the three Pauli matrices) and $D^\Gamma_{ij}(g)$ is the matrix which represents g in the irreducible representation Γ. Eq.2 allows to obtain from $\hat{\chi}$ a matrix symmetrically adapted with the first row of the representation Γ. The corresponding partners $\hat{\chi}_i^\Gamma$ can be constructed from:

$$\hat{\chi}_i^\Gamma = \sum_g \hat{D}^{E_g}(g)\hat{\chi}_1^\Gamma\hat{D}^{E_g^{-1}}(g)D^\Gamma_{i1}(g) \tag{3}$$

with $i \neq 1$. In this case we found that $\hat{I}$ and $\hat{\sigma}_y$ transform in agreement with A_{1g} and A_{2g} respectively. While $\hat{\sigma}_z$ transforms in agreement with the first row of E_g and $\hat{\sigma}_x$ is its partner. To determine the matrices symmetrically adapted with E_g we chose $(k_x^2 - k_y^2, 2k_xk_y)$ as basis for the construction of $\hat{D}^{E_g}(g)$.

At this point, for each irreducible representation Γ, we can construct the corresponding invariant ($\mathcal{T}_\Gamma$) as a product of symmetrically adapted matrices $\hat{\chi}_i^\Gamma$ and irreducible tensor components $\mathcal{K}_i^\Gamma$: $\hat{\mathcal{T}}^\Gamma = \sum_i \hat{\chi}_i^\Gamma\mathcal{K}_i^\Gamma$.

In particular we obtain two invariants: $\hat{\mathcal{T}}^{A_{1g}} = \hat{I}(k_x^2 + k_y^2)$ and $\hat{\mathcal{T}}^{E_g} = \hat{\sigma}_z(k_x^2 - k_y^2) + 2\hat{\sigma}_x k_x k_y$ but we do not find

any invariant transforming with the A_{2g} representation. This happens because at the second order the tensor operator $\mathcal{K}$ does not contain any term belonging to the A_{2g} representation (see table I). On the other hand, in the presence of a magnetic field along the Z axes (H_z), one other term gL_zH_z appears in the Hamiltonian (L_z being the Z component of the angular momentum) which results in a third tensor operator related to the commutator $[k_x, k_y]$ and belonging to the A_{2g} representation. As a consequence a third invariant $\hat{\mathcal{T}}^{A_{2g}} \propto \hat{\sigma}_y[k_x, k_y]$ appears in the Hamiltonian.

Thus, each liner combination of the two invariants $\hat{\mathcal{T}}^{A_{1g}}$ and $\hat{\mathcal{T}}^{E_g}$ satisfies by construction Eq. 1, so that the correct form of the $\mathbf{k}\cdot\mathbf{p}$ Hamiltonian is:

$$\hat{H}(\mathbf{k}) = \alpha\hat{I}(k_x^2 + k_y^2) + \beta[\hat{\sigma}_z(k_x^2 - k_y^2) + 2\hat{\sigma}_x k_x k_y] \quad (4)$$

with two independent parameters α and β. Diagonalizing Eq.4 we find that the band dispersion in $\mathbf{k}$ space is spherically symmetric with $E(\mathbf{k}) = (\alpha \pm \beta)(k_x^2 + k_y^2)$. On the other hand for the conduction band we found the trivial result: $\hat{H}(\mathcal{K}) = \frac{k_x^2+k_y^2}{2m_e}$.

Moreover, from the calculation of α ($\alpha = -1.31/m_0$), β ($\beta = -0.49/m_0$) and m_e ($m_e = 0.83m_0$) by interpolating the ab-initio band structure (Fig.1) we found the mean value of the effective mass of the two nearly degenerate excitons close to $\mu_{ex} = 0.29\ m_0$ (m_0 being the electron mass).

[1] P. Hohemberg and W. Kohn, *Phys. Rev.* **136**, B864 (1964).
[2] W. Kohn and L. J. Sham, *Phys. Rev.* **140**, A1133 (1965).
[3] J. P. Perdew and A. Zunger, *Phys. Rev.* B **23** 5048 (1981).
[4] S. Baroni, A. Dal Corso, S. de Gironcoli and P. Giannozzi, http://www.pwscf.org.
[5] G. Bachelet, D. R. Hamann and M. Schlüter, *Phys. Rev.* B **26**, 4199 (1982).
[6] H. J. Monkhorst and J. D. Pack, *Phys. Rev.* B **13**, 5188 (1976).
[7] R. P. Feynmann, *Phys. Rev.* **56**, 340 (1939).
[8] J. O. Sofo, A. S. Chaudhari and G. D. Baber, *Phys. Rev. B* **75**, 153401 (2007).
[9] D. W. Boukhvalow, M. I. Katsnelson and A. I. Lichtenstein, *Phys. Rev.* B **77**, 035427 (2008).
[10] S. Baroni, S. de Gironcoli, A. Dal Corso and P. Giannozzi, *Rev. Mod. Phys.* **73**, 515 (2001).
[11] L. Hedin and S. Lundquist, *Solid State Physics*, edited by H. Ehrenreich, F. Seitz and D. Turnbull (Academic, New York, 1969), Vol. 23, p. 1.
[12] A. Marini, C. Hogan, M. Grüning and D. Varsano, *Computer Physics Communications* **180**, 1392 (2009).
[13] G. Onida, L. Reining and A. Rubio, *Rev. Mod. Phys.* **74**, 601 (2002).
[14] G. L. Bir and G. E. Pikus, *Symmetry and strain-induced effects in Semiconductors*, (Wiley, New York), 1974.